Nuclear Physics **A401** (1983) 1–21

THE MOMENTS OF STRENGTH FUNCTIONS

G.G. DUSSEL*, R.P.J. PERAZZO*, S.L. REICH and H.M. SOFÍA

Departamento de Física, Comisión Nacional de Energía Atómica, 1429 Buenos Aires, Argentina

Received 26 November 1982

Abstract: In this paper we show that a moment of order n of the strength function is determined by the same order of the Brillouin–Wigner perturbative expansion. This fact is used to study the second moment for single-particle and collective excitations in the framework of nuclear field theory. We discuss the relationship of the second moment with the spreading width of the giant isovector M1 resonances in ^{208}Pb.

1. Introduction

The promotion of nucleons across the Fermi surface to unnoccupied major valence shells gives rise to giant multipole resonances that are coherent particle–hole excitations that exhaust a great portion of the sum rule for a multipole electric or magnetic operator. These states can be pictured macroscopically as a collective oscillation of the nuclear surface and appear as strong peaks in the cross sections of photoabsorption and inelastic scattering of alphas, ^{3}He or protons.

The centroid of those distributions of multipole strength, or what is the same, the excitation energy of the corresponding collective states, can be accounted for within [1]) a microscopic framework performing RPA calculations with either model or effective interactions. Alternatively, a macroscopic description can be attempted within the liquid drop model. Both approaches successfully reproduce the extensive experimental [2,3]) evidence gathered so far, making it possible to link each specific giant mode with the corresponding terms appearing in the residual nucleon–nucleon interaction.

The distribution of fragments of multipole strength gauge the damping of the collective oscillation by its decay into the more complicated nuclear configurations that appear at such excitation energies. This coupling cannot be calculated within the framework of the RPA since it involves higher-order admixtures of configurations with 2p-2h, 3p-3h, etc.

The experiments of one-particle transfer also display similar features. Usually one strong peak gives the position of the so-called single-particle state but weaker peaks associated to states of the same spin and parity ordinarily appear shaping up a distribution of one-body transfer strength that is not a simple delta-type

* Member of the Consejo Nacional de Investigaciones Científicas y Técnicas, Buenos Aires, Argentina.

function. The centroid of the distribution can be calculated in terms of an average one-body central (Hartree–Fock (HF)) potential but its width can only be calculated if some coupling is introduced between pure single-particle excitations and more complicated configurations.

From the above considerations, we can observe that both situations bear a strong resemblance. In both cases the centroid of the strength distribution is described by HF or RPA and its spreading width by the coupling of these excitations to more complicated configurations of the A-nucleon system.

To describe the spreading width of both kinds of excitations several theoretical attempts have been made [1–12]). The general structure of these calculations involves the choice of an appropriate set of intermediate (or doorway) states to which the decaying state is coupled. An averaging procedure is next followed replacing the discrete set of intermediate states by a superposition of continuous Breit–Wigner distributions. This procedure is equivalent to adding a (small) imaginary part to the unperturbed energies of the intermediate states. The coupling to these is then reflected in a width parameter [14]) Γ of the strength distribution that is thus obtained.

The purpose of the present paper is to describe the damping of a giant resonance by the value of the second moment $\mu^{(2)}$ of its strength distribution. The parameter $\mu^{(2)}$ is different from the width Γ [refs. [10,14])] that provides a direct measure of the lifetime of the state. The second moment provides instead an overall measure of the leading order admixtures of the collective mode with neighbouring, more complicated configurations.

The derivations of the present paper are performed within nuclear field theory [13]) assuming that all the strength is concentrated in a single collective state and no distribution of intensity is present in any different RPA (or TDA) modes [25]).

In the following sections we investigate in some detail the physical information that can be extracted from the calculation of a given moment of either a single-particle or a particle–hole strength distribution discussing in each case the set of intermediate states that determines it uniquely. We next analyze within this framework the realistic situation of the isovector M1 giant resonance in ^{208}Pb. In the last section we draw conclusions and compare these with other frameworks.

2. The single-particle case

Let $\boldsymbol{H}$ be a hamiltonian matrix with elements h_{ij} and $\boldsymbol{U}$ the unitary matrix that brings $\boldsymbol{H}$ to its diagonal form with eigenvalues E_i. The matrix $\boldsymbol{U}$ is built by the eigenvectors of $\boldsymbol{H}$. Then the following equations hold

$$\boldsymbol{HU} = \boldsymbol{UE}\,, \qquad \boldsymbol{U}^{\mathrm{T}}\boldsymbol{U} = \boldsymbol{1}\,,$$

$$\sum_i h_{ij}u_{jk} = u_{ik}E_k\,, \tag{1}$$

and thus

$$\boldsymbol{H} = \boldsymbol{U}\boldsymbol{E}\boldsymbol{U}^{\mathrm{T}} = \boldsymbol{M}(\boldsymbol{E}),$$

$$h_{ii} = \sum_k (u_{ik})^2 E_k = \sum_k u_{ik} E_k u_{ki}^* . \tag{2}$$

Eq. (2) is just an energy-weighted sum rule for the eigenvector components u_{ik} relating the unperturbed energies contained in h_{ii} to the final eigenvalues E_k.

To make clear the physical meaning of eq. (2) suppose that a complete set of single-particle states with unperturbed energies ε_i has been defined through a HF self-consistent diagonalization. Next we introduce in our basis more complicated 2p-1h (or equivalently one-particle + one-boson) states and ask ourselves what will be the effect of the coupling to these states through the residual interaction contained in $\boldsymbol{H}$. We see through eq. (2) that the weighted average of the final eigenvalues is given by the diagonal matrix element h_{ii} that is composed only by the bare single-particle energy ε_i. In addition the square of the eigenvector components are the amplitudes of exciting 2p-1h states by a process of one-particle transfer and are thus interpreted as one-body spectroscopic amplitudes. We thus see that the coupling to 2p-1h configurations causes a redistribution of one-particle strength but its envelope is still centered at the unperturbed value ε_i. The introduction of the 2p-1h states changes in fact the next moment of the strength distribution through the off-diagonal terms of the hamiltonian matrix. To see this we note that

$$(\boldsymbol{H}^2) = (\boldsymbol{U}\boldsymbol{E}\boldsymbol{U}^{\mathrm{T}}\boldsymbol{U}\boldsymbol{E}\boldsymbol{U}^{\mathrm{T}}) = (\boldsymbol{U}\boldsymbol{E}^2\boldsymbol{U}^{\mathrm{T}}) = \boldsymbol{M}(\boldsymbol{E}^2) . \tag{3}$$

Thus the second moment associated with the ith unperturbed state is

$$\mu_i^{(2)} = (\boldsymbol{U}\boldsymbol{E}^2\boldsymbol{U}^{\mathrm{T}})_{ii} - (\boldsymbol{U}\boldsymbol{E}\boldsymbol{U}^{\mathrm{T}})_{ii}^2 = \sum_{k\neq i} h_{ki}^2 . \tag{4}$$

It is conceptually helpful to work out a perturbative interpretation of $\mu_i^{(2)}$ and of higher moments. For this purpose we analyze the Brillouin–Wigner (BW) perturbative expansion of the state $|0\rangle$ with energy ε_0. This amounts to solving the equation

$$E = f_0(E) , \tag{5}$$

with

$$\begin{aligned} f_0(E) &= \varepsilon_0 + \langle 0|V\frac{1}{E-H_0}(1-|0\rangle\langle 0|)V|0\rangle \\ &\quad + \langle 0|V\frac{1}{E-H_0}(1-|0\rangle\langle 0|)V\frac{1}{E-H_0}(1-|0\rangle\langle 0|)V|0\rangle + \cdots \\ &= \varepsilon_0 + \sum_{k\neq 0}\frac{V_{0k}^2}{E-\varepsilon_k} + \sum_{\substack{k\neq 0\\ r\neq 0}}\frac{V_{0k}V_{kr}V_{r0}}{(E-\varepsilon_k)(E-\varepsilon_r)} + \cdots . \end{aligned} \tag{6}$$

In (6) we have assumed that the hamiltonian splits into an unperturbed (diagonal) part H_0 and a perturbation V that couples the state $|0\rangle$ to more complicated configurations $k, r \cdots$. We have further assumed that any diagonal contribution V_{00} has been already absorbed in ε_0.

It can clearly be seen by straightforward application of the Cauchy theorem that

$$\mu_0^{(2)} = \frac{1}{2\pi i} \int_C f_0(z)\, dz = \sum_{k \neq 0} V_{0k}^2 , \tag{7}$$

where C is a closed contour in the complex energy-plane that encircles all eigenvalues of H_0.

We thus conclude that $\mu_0^{(2)}$ is uniquely determined by the second (in powers of V) order in the BW perturbative expansion. We can extend this argument to the third-order moment, namely

$$\begin{aligned} \mu_0^{(3)} &= \boldsymbol{M}((\boldsymbol{E} - \boldsymbol{M}(\boldsymbol{E}))^3) \\ &= \sum_{j \neq 0} V_{0j}^2 (\varepsilon_j + V_{jj} - \varepsilon_0) + \sum_{k,j \neq 0} V_{0j} V_{jk} V_{k0} \\ &= (\boldsymbol{U}\boldsymbol{E}^3\boldsymbol{U}^{\mathrm{T}})_{00} - 3(\boldsymbol{U}\boldsymbol{E}^2\boldsymbol{U}^{\mathrm{T}})_{00}(\boldsymbol{U}\boldsymbol{E}\boldsymbol{U}^{\mathrm{T}})_{00} + 2(\boldsymbol{U}\boldsymbol{E}\boldsymbol{U}^{\mathrm{T}})_{00}^3 . \end{aligned} \tag{8}$$

This expression can be found to be equal to

$$\mu_0^{(3)} = \frac{1}{2\pi i} \int_C (z - \varepsilon_0) f_0(z)\, dz . \tag{9}$$

The only non-vanishing contributions to the integral in (9) come from the second and third terms of (6). Formulae (7) and (9) can of course be generalized to higher moments. The main conclusion that we want to remark is that a moment of a given order is properly calculated upon the inclusion of all the terms in the BW perturbative expansion up to that same order. This allows to cast the calculation of moments into a diagrammatic language by simply identifying the set of processes that are relevant to a given set of terms in the BW expansion.

For the single-particle case that is under consideration we have seen that the coupling to 2p-1h states does not change the centroid. In addition the distribution of one-particle transfer strength given by the squares of the components of the eigenvectors is no longer concentrated but is instead distributed being enveloped by a gaussian with a width determined by the non-vanishing $\mu^{(2)}$. Its value is *only* given by the sums of the squares of the matrix elements that couple 1p to 2p-1h states.

This coupling can be evaluated using as elementary modes of excitation 1p states and coherent particle–hole modes. As long as we restrict our analysis to TDA bosons, it is easy to see that

$$\begin{aligned} \mu_k^{(2)} &= \sum_{2\mathrm{p1h}} |\langle (1\mathrm{p})|V|(2\mathrm{p1h})\rangle|^2 = \sum_{k',i,k''} \langle ki|V|k'k''\rangle\langle k'i|V|kk''\rangle \\ &= \sum_{k',n} \Lambda(k'k, n)\Lambda(kk', n) \qquad (k, k' \rangle j_{\mathrm{Fermi}};\ i, i' < j_{\mathrm{Fermi}}) , \end{aligned} \tag{10}$$

where [13])

$$\Lambda(j_a j_b, n) = \sum_{jj'} \langle j_a j | V | j_b j' \rangle \lambda^{n}_{jj'} . \tag{11}$$

In eqs. (10) and (11) $\Lambda(j_a j_b, n)$ are the vertex functions coupling two fermions in states $j_a j_b$ to a TDA boson labelled by n; $\lambda^{n}_{jj'}$ are the eigenvectors components of the nth boson in the jj' (p-h) configuration.

Not all the diagrams having a fermion line as initial state and a fermion plus a boson lines as a final state represent matrix elements that contribute to $\mu^{(2)}$. For instance, diagrams such as those of (fig. 1B) renormalize the vertex Λ (or equivalently the two-body matrix element of V) introducing higher-order corrections in the structure of the correlated p-h states. The arguments leading to eq. (10) exclude their contributions to $\mu^{(2)}$ despite the fact that they represent matrix elements connecting the same initial and final states (e.g. 1p and 2p-1h). Equivalently they must be neglected because they correspond to higher orders in the BW expansion.

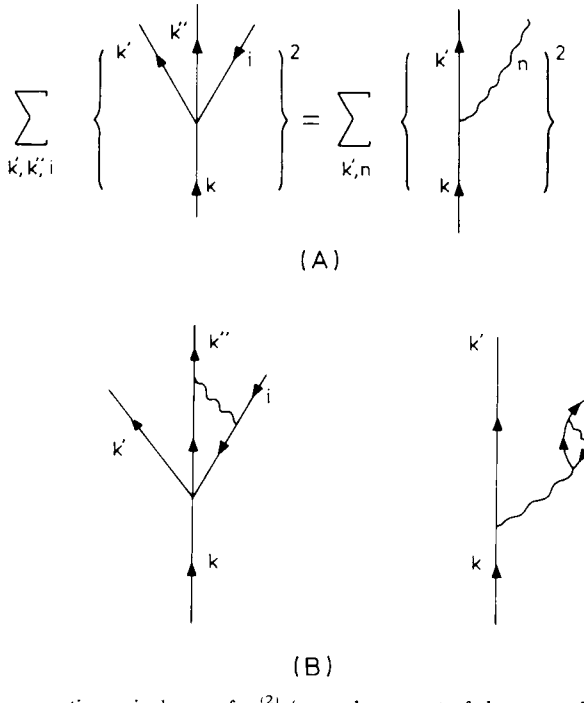

Fig. 1. (A) Diagrammatic equivalence of $\mu^{(2)}_k$ (second moment of the strength function of the single fermion k) calculated within a basis of independent particles and holes and a basis spanned by single particles and TDA bosons. In this and following figures wavy lines represent bosons and full lines single particles (or holes). The two-body matrix element $\langle k'k''|V|ki\rangle$ (including direct and exchange parts) is represented by a dot. The particle-boson vertex is $\Lambda(k'k, n)$. (B) Higher-order renormalizations of the two-body matrix element (or vertex function) that do not contribute to $\mu^{(2)}_k$.

The calculations of widths of s.p. states can therefore be achieved in a much more simple way not going through a TDA diagonalization since the summation of the Λ's over all (collective and non-collective) modes is equal to the sum of the squares of the corresponding p-h matrix elements (see fig. 1A).

More complicated configurations entering in higher orders of the BW expansion only change higher-order moments. This amounts to stating that the details of the strength distribution will change upon the inclusion of such terms but in such a way that the average gaussian envelope remains the same. This is schematically displayed in fig. 2.

3. The particle–hole case

The arguments of the preceding section can also be extended to the strength function associated with a collective particle–hole excitation. We will restrict our discussion to the case in which coherent p-h modes are described within the TDA.

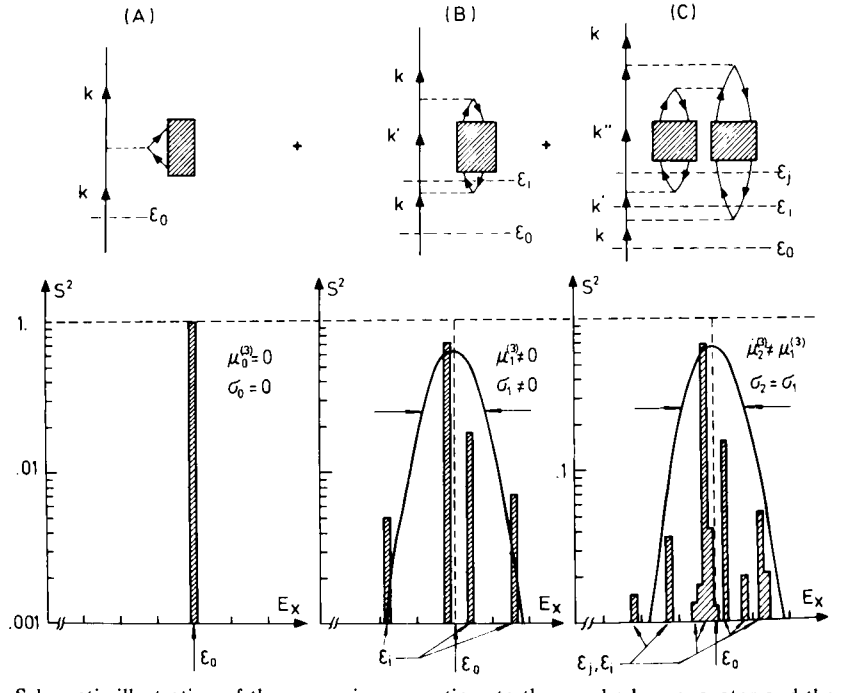

Fig. 2. Schematic illustration of the successive corrections to the one-body propagator and the corresponding fragmentation of the strength function. (A) The zeroth order in the BW expansion corresponds to the diagrams shown in the upper part that have only one insertion in the fermion line and there is no fragmentation in the strength function (below). The second and third moments are zero ($\sigma_0=\mu_0^{(3)}=0$). (B) The next order involves diagrams with two insertions. Some strength is transferred to the intermediate configurations with energies ε_i. These are enveloped by a gaussian with a width given by $\sigma_1\neq 0$. The third moment is also different from zero. (C) The further corrections that involve diagrams with three insertions change the details of the strength distribution; the width σ remains unchanged ($\sigma_2=\sigma_1$) but $\mu^{(3)}$ changes. Higher corrections leave $\mu^{(3)}$ unchanged.

The energy-weighted sum rule given in eq. (2) can be applied straightforwardly. However since h_{ii} contains an important diagonal contribution, the centroid of bare particle–hole energies is different from that of the TDA eigenenergies. The fact that these centroids are not the same can easily be seen in the schematic models in which a single (collective) eigenstate is strongly shifted downwards (upwards) for an attractive (repulsive) two-body interaction, while all non-collective modes remain degenerate at their unperturbed energies.

The TDA diagonalization must therefore be regarded in a similar way as the HF calculation in the sense that both are the initial steps that define the excitation energies (centroids) of the configurations that are used as building blocks to construct the nuclear spectrum.

The situation, that is comparable to the corrections discussed in sect. 2 for the one-particle configurations, is that arising from the admixture of 2p-2h, 3p-3h, etc. with a coherent 1p-1h state.

To study this admixture it is conceptually advantageous to work in a basis of TDA quasibosons (in what follows bosons). We thus define

$$|n\rangle = \sum_{(ki)} \lambda^{n}_{ki} |ki\rangle = \sum_{(ki)} \lambda^{n}_{ki} c^{+}_{k} c_{i} |0\rangle \,. \tag{12}$$

In eq. (12) k (i) labels a state above (in) the Fermi sea and $|0\rangle$ is the HF vacuum. Within this scheme the basis is built up by states of 1, 2, 3, etc. bosons:

$$|n\rangle \quad ; \quad |n_1 n_2\rangle \quad ; \quad |n_1 n_2 n_3\rangle \quad ; \quad \cdots . \tag{13}$$

The states of 2 or more bosons do not correspond to fully antisymmetric states of 4, etc. fermions since Pauli exchange effects are neglected. This happens because a given single-particle state can simultaneously be occupied by a particle (or hole) that participates in the structure of two different bosons. The results thus obtained are wrong in terms of the order $1/\Omega$ where Ω stands for the effective degeneracy of all the valence orbitals involved in the calculation. This error can be corrected by taking into account the fact that the missing $1/\Omega$ corrections introduce a non-orthogonality of the many boson states in the basis (13). This can be corrected by introducing the matrix of the overlaps of these states, very much in the style of the multistep shell-model method [24]). This is however a technical point that does not affect the following arguments and is ignored in the discussion that follows.

According to eq. (13) the second moment of a given (collective) boson state $|n_0\rangle$ is given by

$$\mu^{(2)}_{n_0} = \sum_{r \neq 1} |\langle n_0 | H | n_1 n_2 \ldots n_r \rangle|^2 \,. \tag{14}$$

The summation is extended over states of more than one boson since the TDA diagonalization is assumed to leave the one boson part of the hamiltonian matrix in its diagonal form.

The r-boson portion of the basis (13) is an (overcomplete) image only of states of r particles and r holes. As we have seen already, the only contributions to $\mu^{(2)}$ are due to all the matrix elements involving the first power of the two-body interaction and having $|n_0\rangle$ as initial state. Since these can only connect $|n_0\rangle$ with states of two particles and two holes, the summation in (14) is restricted to $r = 2$. The only matrix element that survives is

$$\langle n_1 n_2|H|n_0\rangle = \sum_{\substack{k's \\ i's}} \lambda^{n_1}_{k_1 i_1} \lambda^{n_2}_{k_2 i_2} \lambda^{n_0}_{k_0 i_0} \langle (k_1 i_1)(k_2 i_2)|H|(k_0 i_0)\rangle \,. \tag{15}$$

This can be written as

$$\langle n_1 n_2|H|n_0\rangle = \Big\{ \sum_{kk'i} \lambda^{n_1}_{k'i} \lambda^{n_0}_{ki} \Lambda(k'k; n_2) + \lambda^{n_2}_{k'i} \lambda^{n_0}_{ki} \Lambda(k'k; n) + \sum_{kii'} \lambda^{n_1}_{ki'} \lambda^{n_0}_{ki} \Lambda(i'i; n_2) + \lambda^{n_2}_{ki'} \lambda^{n_0}_{ki} \Lambda(i'i; n_1) \Big\} (1+\delta_{n_1 n_2})^{-1/2} \,. \tag{16}$$

In eq. (16) is defined an energy-independent vertex between one- and two-boson states. Each of the four terms is diagrammatically represented in fig. 3B. In performing all possible contractions in (15) to obtain (16) the RPA-type vertices have been assumed to be zero, thus the only contributions arise from matrix elements of the type shown in fig. 3A.

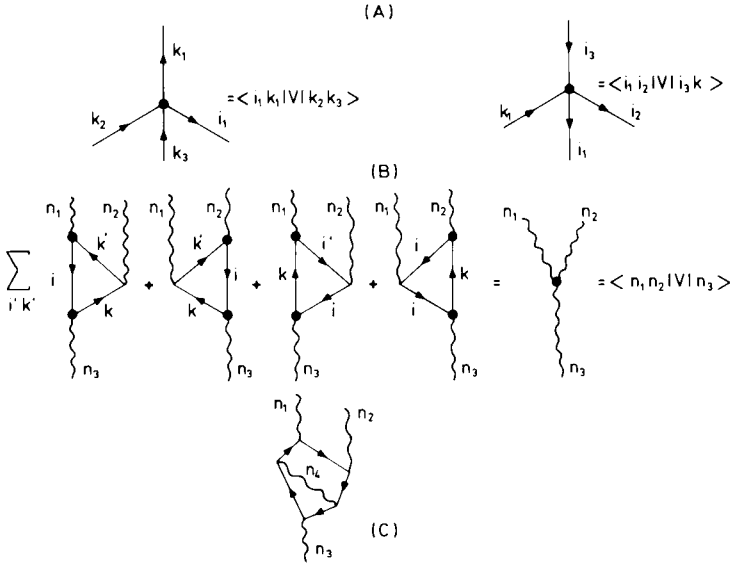

Fig. 3. (A) Two-body matrix elements (including direct and exchange parts) that are relevant to the admixture of one and two TDA bosons. (B) Diagrammatic representation of eq. (16) in the text. Heavy dots represent the amplitudes λ. The remaining vertices are given by Λ (as in fig. 1) as defined in eq. (11). (C) Higher-order renormalization of the matrix element (15) that gives no contribution to $\mu^{(2)}$.

The processes such as the one shown in fig. 3C give no contribution to $\mu^{(2)}$ despite the fact that they represent a matrix element between one- and two-boson states. The reason for this is that the diagram involves a higher power of V and therefore corresponds to a higher order in the BW expansion of the boson state $|n_0\rangle$. This type of renormalization is to be compared with that of fig. 1B for the case of one-particle states.

With the arguments of this section we have obtained, in a similar fashion to the preceding one, the family of all the states whose admixture determines completely the second moment of the strength distribution of a TDA boson.

4. A schematic model for the particle–hole case

In this section we check the adequacy of the vertex function (16) in a schematic model. We do this by using (16) in a hamiltonian matrix to calculate by diagonalization the perturbed energy of one boson. The correction to the TDA frequency ω obtained in this way is correct up to order $1/\Omega$[+]. The results obtained from this diagonalization can be checked against a perturbative calculation that can be made exact up to any required order in $1/\Omega$ following the prescriptions of ref. [13]).

We consider a model consisting of two levels labelled σ and $\bar{\sigma}$ of the same degeneracy Ω and separated by an energy gap ε. Identical particles are assumed to fill completely the lower level. They are assumed to interact via a monopole two-body interaction. The only non-zero two-body matrix elements are shown in fig. 4. The TDA diagonalization (in which the exchange matrix elements shown in fig. 4D have been neglected) yields a single collective state at an excitation energy

$$\omega = \varepsilon - 2V\Omega = \varepsilon(1-x)\,. \tag{17}$$

The only non-vanishing matrix element occurs between the states with one and two adiabatic bosons. The 2Ω coefficients $\lambda_{\sigma\bar{\sigma}}$ are equal to $1/\sqrt{2\Omega}$. The four diagrams in fig. 3B are thus equal in pairs. The different sign for the clockwise or counter clockwise orientation of the fermion lines of each group is contained in the q_σ $(-q_{\bar{\sigma}})$ factor. The admixture of one- and two-boson states is then described by the two-by-two matrix

$$\begin{vmatrix} \omega - Vq_\sigma q_{\bar{\sigma}} & -\Lambda\sqrt{2}(q_\sigma - q_{\bar{\sigma}}) \\ -\Lambda\sqrt{2}(q_\sigma - q_{\bar{\sigma}}) & 2(\omega - Vq_\sigma q_{\bar{\sigma}}) \end{vmatrix}, \tag{18}$$

with $\Lambda = \varepsilon x/\sqrt{2\Omega}$.

Besides the unperturbed energies ω and 2ω, the diagonal matrix elements contain the exchange contribution $Vq_\sigma q_{\bar{\sigma}}$. The lowest eigenvalue is shifted by an amount

$$\delta\omega = -\left\{\frac{\varepsilon x^2 (q_\sigma - q_{\bar{\sigma}})^2}{\Omega(1-x)} + \frac{\varepsilon x q_\sigma q_{\bar{\sigma}}}{2\Omega}\right\} + O(\Omega^{-2})\,. \tag{19}$$

[+] Corrections of order $1/\Omega$ are missing in the wave function of the two-boson state. These cause eigenvalues to be wrong in terms of order $1/\Omega^2$.

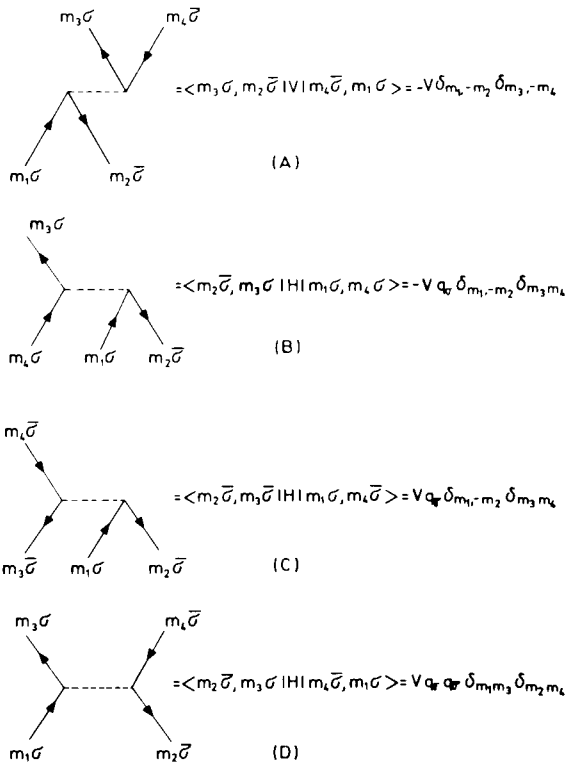

Fig. 4. Two-body matrix elements of the monopole p-h interaction. Backward matrix elements are set equal to zero.

This same correction can be calculated in perturbation theory. This amounts to evaluating the nine different contributions represented by the diagrams of fig. 5. These are

$$D_1 = -Vq_\sigma q_{\bar\sigma}\frac{\Lambda^2 2\Omega}{(\omega-\varepsilon)^2},$$

$$D_2 + D_3 = \frac{2\Omega\Lambda^4(q_\sigma - q_{\bar\sigma})^2}{(\omega-\varepsilon)^2(-\varepsilon)},$$

$$D_4 = \frac{4\Omega^2 V^2\Lambda^2(q_\sigma - q_{\bar\sigma})^2}{(\omega-\varepsilon)^2(\omega-2\varepsilon)},$$

$$D_{5(a)} + D_{5(b)} = \frac{4\Omega^2 V\Lambda^4(q_\sigma - q_{\bar\sigma})^2(4\varepsilon-\omega)}{(\varepsilon-\omega)^2(\omega-2\varepsilon)\varepsilon^2},$$

$$D_{6(a)} + D_{6(b)} + D_{6(c)} = \frac{4\Omega^2\Lambda^6(4\varepsilon-\omega)(q_\sigma - q_{\bar\sigma})^2}{(\omega-2\varepsilon)(\varepsilon-\omega)^2\varepsilon^2\omega}. \qquad (20)$$

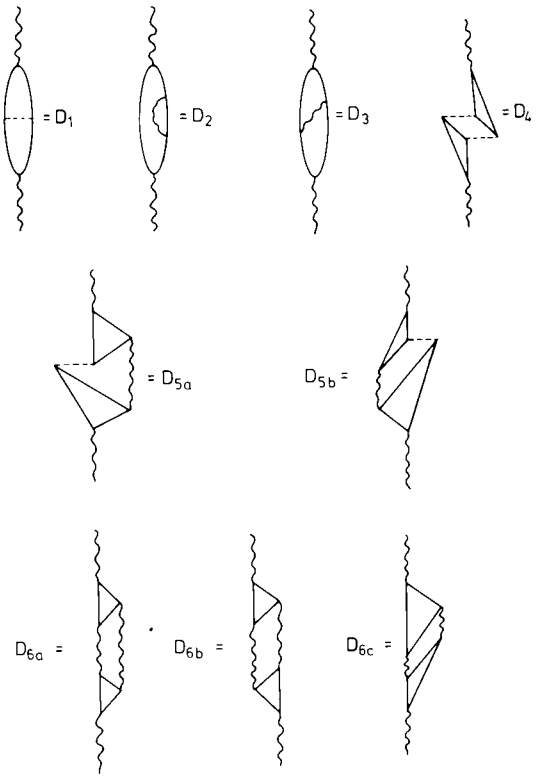

Fig. 5. Diagrammatic representations of the $1/\Omega$ anharmonicities of the one- (TDA) boson state. Fermion lines are drawn with no arrows to indicate that clockwise and counter-clockwise orientations should be included. Their evaluation is given in eqs. (20). The dotted lines represent the exchange part of the two-body interaction.

The partial contributions (20) can be checked to add to the result obtained in (19) from the diagonalization of (18). This comparison shows in a striking way the adequacy of the matrix element (16). In fact the inclusion of this coupling is surprisingly able to account for all the variety of different diagrams of fig. 5. The obvious consequence as far as the calculation of second moments is concerned is that the $\lambda\lambda\Lambda$ term takes into account *all* possible fragmentations of the one-boson state in all possible two-boson configurations. In the next subsection we analyze this procedure in a realistic situation.

5. The isovector M1 resonance in ^{208}Pb

The isoscalar or isovector M1 resonance in closed-shell nuclei occurs whenever it is possible to create particle–hole excitations that have a non-vanishing matrix element of the operator $\boldsymbol{\sigma}$ ($\boldsymbol{\sigma\tau}$) with the g.s. This occurs whenever two spin-orbit

partner orbitals lie one above and one below the Fermi surface, i.e. when a spin-unsaturated shell closure occurs [15]).

Despite the large effort put in this measurements to overcome severe experimental difficulties there is still some degree of uncertainty in the total M1 strength located at an excitation energy of the order of the spin-orbit splitting between the particle and hole levels. The experimental evidence is however consistent in showing that only a small fraction of the expected M1 strength is detected thus indicating a quenching of the σ-operator.

The extensive experimental work [16]) in the $T = 1$, M1 state in ^{208}Pb has resulted in high-resolution information of many fragments of M1 strength. This fact together with the simplicity of the structure of the 1^+ state makes this case particularly suitable for applying the methods presented in sect. 3. Several microscopic descriptions have been attempted within various frameworks [17]) and with a wide variety of residual interactions. We are not attempting here an alternative version of them but rather provide an analysis of the mechanisms of the fragmentation of the M1 state.

In this section we will first reproduce the experimental evidence within a phenomenological RPA calculation and next calculate the width of the state following the prescription of sect. 3. To describe the 1^+ state we use the model (factorizable) interaction

$$V(1,2) = \sqrt{\tfrac{1}{3}} K_{\mathrm{M}} \sum_{\mu} (-)^{1-\mu} \sigma_{\mu}(1) \sigma_{-\mu}(2) \tau_z(1) \tau_z(2) . \tag{21}$$

The strength K_{M} is chosen to reproduce the centroid ω_{1^+} of the M1 distribution. The proton (π) and neutron (ν) configurations that are involved are $[(h_{11/2})^{-1}(h_{9/2})]^{1^+}$ and $[(i_{13/2})^{-1}(i_{11/2})]^{1^+}$ together with the corresponding backward amplitudes. Thus

$$B(\mathrm{M1}; 0^+_{\mathrm{g.s.}} \to 1^+) = |\langle 1^+ \| \mathrm{M1} \| 0 \rangle|^2$$

$$= \Lambda_{1^+}^2 \frac{3\mu^2}{4\pi} \left\{ (g_s - g_l)_{\nu} \frac{4l_{\nu}(l_{\nu}+1)}{2l_{\nu}+1} - (g_s - g_l)_{\pi} \frac{4l_{\pi}(l_{\pi}+1)}{2l_{\pi}+1} \right\}^2 \left(\frac{2\bar{\varepsilon}}{\bar{\varepsilon}^2 - \omega_{1^+}^2} \right)^2 , \tag{22}$$

$$\Lambda_{1^+} = R \left\{ \sum_{ki} |\langle k \| \boldsymbol{\sigma} \| i \rangle|^2 \frac{2\varepsilon_{ki}\omega_{1^+}}{\varepsilon_{ki}^2 - \omega_{1^+}^2} \right\}^{-1/2} . \tag{23}$$

In (22) $\bar{\varepsilon}$ is the average between the proton and neutron particle–hole energies, and in (23), $\varepsilon_{ki} = \varepsilon_k + \varepsilon_i$ (we take positive particle and hole s.p. energies). R is a renormalization factor that is chosen to reproduce the total M1 strength measured. This renormalization can be thought of as mocking up effective gyromagnetic ratios or, equivalently, coupling to the Δ-hole configurations [18,19]).

The residual hamiltonian (21) has been chosen to be proportional to the square of an operator that is very close to the specific operator for the M1 transition. This

choice insures that the collective RPA root concentrates all the strength and thus no fragmentation is present among the remaining RPA roots. The fragments of M1 strength are thus obtained by calculating in the lowest perturbative order the amplitudes of exciting a two-boson state $|n_1J_1, n_2J_2; 1^+\rangle$ by acting with the M1 operator over the ground state. We do this following the rules of nuclear field theory [13]), i.e. by evaluating the diagrams represented in fig. 6. As can be seen both the "collective" (fig. 6A, D, E) and "fermionic" (fig. 6B, C) images of the M1 operator have to be considered. In fig. 6 we have omitted for simplicity all the remaining possible time permutations that have to be considered if all the phonons are described within the RPA.

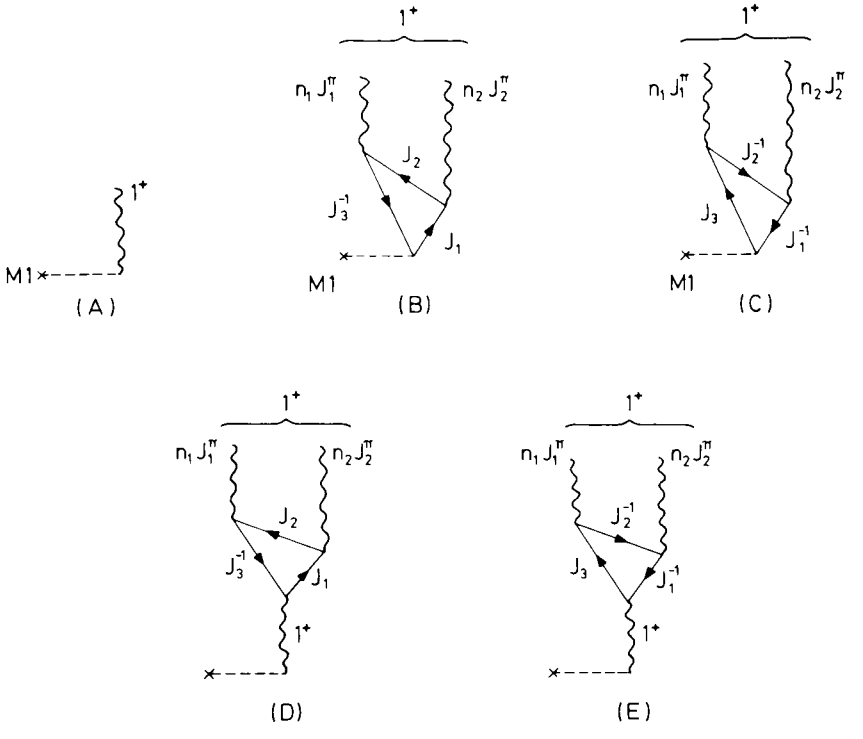

Fig. 6. Diagrams representing the processes responsibles of the population of one- and two-boson states via an M1 excitation. The only time permutation that is shown corresponds to a TDA description of the boson state.

The fermionic lines are taken to represent particle or hole states for both protons and neutrons belonging to one major shell above or below the Fermi surface. The corresponding s.p. energies are taken from the ^{208}Pb odd neighbouring isotopes.

The boson states labelled $|n_iJ_i\rangle$ are any of the RPA roots of a separable multipole–multipole interaction of multipolarity J_i acting among protons and neutrons. Written

in terms of isoscalar, isovector and coupling terms [22]),

$$H_J = -\tfrac{1}{2}K_{0,J}\sum_{J_Z} Q^J_{J_Z}(\tau=0,\tau_Z=0)Q^{J^+}_{J_Z}(\tau=0,\tau_Z=0)$$
$$-\tfrac{1}{2}K_{1,J}\sum_{J_Z\tau_Z} Q^J_{J_Z}(\tau=1,\tau_Z)Q^{J^+}_{J_Z}(\tau=1,\tau_Z)$$
$$-K'_J\sum_{J_Z} Q^J_{J_Z}(\tau=1,\tau_2=0)Q^{J^+}_{J_Z}(\tau=0,\tau_Z=0)\,, \tag{24}$$

with

$$Q^J_{J_Z}(\tau,\tau_Z) = 2\sqrt{2}\sum_{t_Z} t_Z\langle \tfrac{1}{2}t_Z\,\tfrac{1}{2}(\tau_Z - t_Z)|\tau\tau_Z\rangle \mathcal{Q}^J_{J_Z}(\tau_Z,t_Z)\,,$$

$$\mathcal{Q}^J_{J_Z}(\tau_Z,t_Z) = -\frac{1}{\sqrt{2J+1}}\sum_{ki}\langle kt_Z\|r^J Y_J\|it_Z\rangle$$
$$\times\{[a^+_{jk\frac{1}{2}t_Z}a_{ji\frac{1}{2}t_Z}]^J_{J_Z} + (-)^{j_k+j_i+J}[a^+_{ji\frac{1}{2}t_Z}a_{jk\frac{1}{2}t_Z}]^J_{J_Z}\}\,. \tag{25}$$

The intensities $K_{0,J}$, $K_{1,J}$ and K'_J are chosen also as in ref. [22]) and are related to the depths V_0 and V_1 of the isoscalar and isovector part of the optical potential through a self-consistent condition between collective fluctuations of the average one-particle potential and the distortion of the density [14,20]):

$$K_{0,J} \simeq \frac{4\pi}{3}\frac{41}{(1.2)^{2J-2}}A^{-(J+3)/3}\left(\frac{M\omega_0}{\hbar}\right)^J \qquad [\mathrm{MeV}]\,, \tag{26a}$$

$$K_{1,J} \simeq -\frac{V_1\pi}{(1.2)^{2J}}\frac{3+2J}{3}A^{-(J+3)/3}\left(\frac{M\omega_0}{\hbar}\right)^J \qquad [\mathrm{MeV}]\,, \tag{26b}$$

$$K'_J \simeq -2K_{1,J}\frac{T_Z}{A}c\,, \qquad 0\leqslant c\leqslant 1\,. \tag{26c}$$

The RPA equations are worked out as in ref. [22]) and yield the frequencies ω_{nJ} and the vertex functions of fig. 7. The normalization constants $\Lambda_{nJ}(t_z)$ are obtained as solutions of the equations

$$[1-(K_{0J}+K_{1J}+2K'_J)]S^{nJ}_+\Lambda_{nJ}(\tfrac{1}{2}) = (K_{0J}-K_{1J})S^{nJ}_-\Lambda_{nJ}(-\tfrac{1}{2})\,,$$
$$[1-(K_{0J}+K_{1J}+2K'_J)]S^{nJ}_-\Lambda_{nJ}(-\tfrac{1}{2}) = (K_{0J}-K_{1J})S^{nJ}_+\Lambda_{nJ}(\tfrac{1}{2})\,, \tag{27}$$

$$S^{nJ}_\pm = \sum_{ki}|\langle kt_Z = \pm\tfrac{1}{2}\|r^J Y_J\|it_Z = \pm\tfrac{1}{2}\rangle|^2\frac{2\varepsilon_{ki}(t_Z)}{\varepsilon^2_{ki}(t_Z)-\omega^2_{nJ}}\,. \tag{28}$$

With these ingredients the diagrams of fig. 6 summed over all time permutations

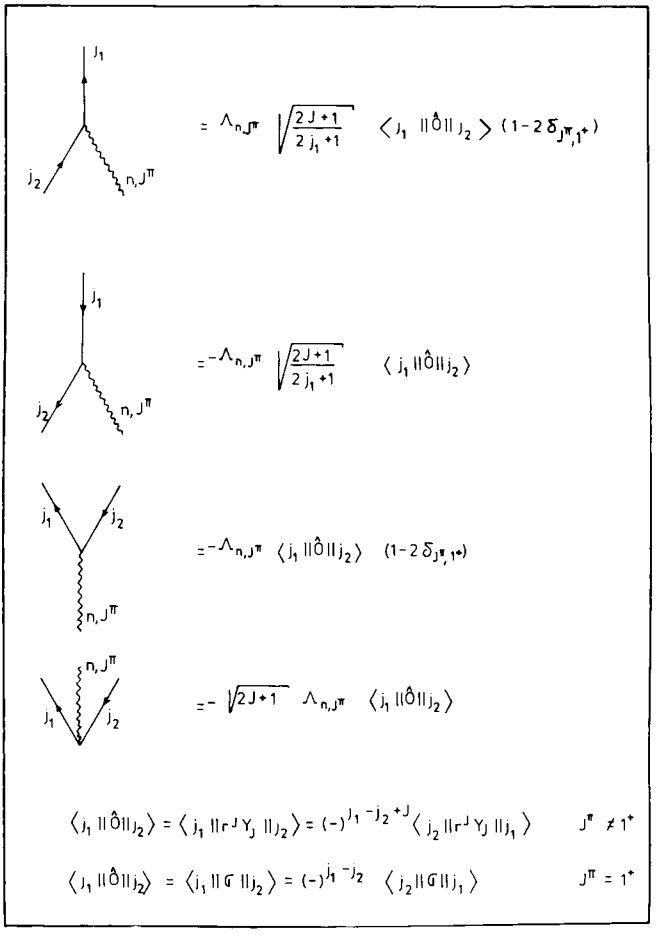

Fig. 7. List of fermion-boson vertices.

give the following M1 transition matrix element:

$$\langle n_1 J_1, n_2 J_2; 1^+ \| \mathrm{M1} \| 0 \rangle = \sum_{j_1 j_2 j_3 t_Z} (-)^{j_1+j_2+J_2} \sqrt{(2J_1+1)(2J_2+1)}$$

$$\times \Lambda_{n_1 J_1}(t_Z) \Lambda_{n_2 J_2}(t_Z) \begin{Bmatrix} J_2 & 1 & J_1 \\ j_3 & j_2 & j_1 \end{Bmatrix} \langle j_3 t_Z \| r^{J_1} Y_{J_1} \| j_2 t_Z \rangle \langle j_1 t_Z \| r^{J_2} Y_{J_2} \| j_2 t_Z \rangle$$

$$\times \left\{ \frac{2\omega_{1^+}}{(\omega_{n_1 J_1} + \omega_{n_2 J_2})^2 - \omega_{1^+}^2} \Lambda_{1^+}(t_Z) \langle j_3 t_Z \| \boldsymbol{\sigma} \| j_1 t_Z \rangle \langle 1^+ \| \mathrm{M1} \| 0 \rangle \right.$$

$$\left. + \langle j_3 t_Z \| \mathrm{M1} \| j_1 t_Z \rangle \right\} \left\{ \frac{1}{(\omega_{n_1 J_1} - \varepsilon_{j_3 j_2}(t_Z))(\omega_{n_1 J_1} + \omega_{n_2 J_2} - \varepsilon_{j_3 j_1}(t_Z))} \right.$$

$$-\frac{1}{(\omega_{n_1J_1}+\varepsilon_{j_3j_1}(t_Z))(\omega_{n_2J_2}-\varepsilon_{j_2j_1}(t_Z))}+\frac{1}{(\omega_{n_2J_2}+\varepsilon_{j_2j_1}(t_Z))(\omega_{n_1J_1}+\omega_{n_2J_2}+\varepsilon_{j_3j_1}(t_Z))}\Bigg\}$$

$$\times\frac{2}{\sqrt{(1+\delta_{n_1n_2}\delta_{J_1J_2})}}. \tag{29}$$

The small energy denominators in (29) that occur in the immediate neighbourhood of the unperturbed energy of the 1^+ boson (7.5 MeV) are handled as usual, through a diagonalisation of a matrix in that restricted space. Although some ambiguities are present in the calculation of the off-diagonal terms these cause no significant effects in the results (e.g. how to symmetrize the matrix).

In addition to the RPA calculation we have performed one within the TDA. This amounts to recalculating not only the 1^+ state but also the p-h excitations that give rise to the fragmentation of the M1 mode. In both cases once the fragments were obtained the second moment was evaluated as if dealing with experimental data, i.e. by using the standard prescription of adding up the products of the M1 intensity in each fragment times the square of the energy distance to the centroid. For this purpose all the low intensity fragments lying further away than 2.5 MeV were neglected. The theoretical results are compared with experiment in fig. 8 and table 1.

All the fragments that are found to be large in the RPA calculation are also found in the experiment at nearly the proper energy. No significant fragments were found more than 1 MeV away from the centroid at 7.5 MeV of excitation energy. The only exceptions are the peaks below 7 MeV that lie below the experimental threshold. Many low intensity fragments that have been measured close to the centroid are missing from the theoretical picture. As long as these can be attributed to more complex configurations than 2p-2h they do not contribute to the value of $\mu^{(2)}$ despite the fact that such weak fragments change the details of the distribution.

The TDA calculation of the width was repeated using the prescription explained in the preceding sections, i.e. by adding up the squares of the matrix elements of eq. (15). The value of σ has been calculated neglecting the contributions due to two-boson states with the excitation energies outside a window of width $\delta\varepsilon$ centred at 7.5 MeV. In fig. 9 the value of σ has been plotted as a function of $\delta\varepsilon$. The value of σ is seen to saturate for increasing $\delta\varepsilon$. This is due first to the fact that the M1 intensity grows weaker for more distant fragments and secondly to the lower number of two-boson configurations available. The asymptotic value of σ is larger than the one quoted in table 1 that was obtained as if dealing with experimental data. This difference is exclusively due to weak and distant fragments that ordinarily cannot be detected experimentally.

In fig. 9 the value of σ is broken up into the contributions of the multipolarities of the bosons that build up the 2p-2h final states. The only configurations that contribute significantly to the fragmentation at low values of $\delta\varepsilon$ involve two 3^- or

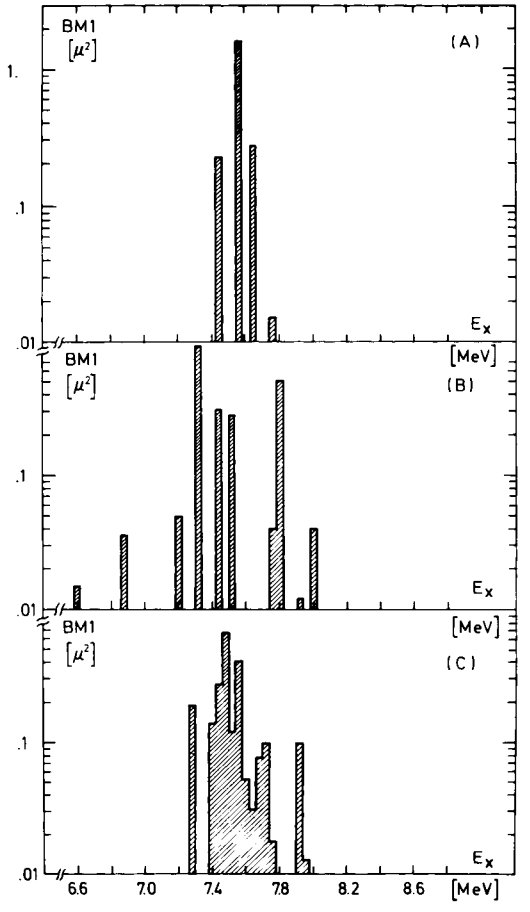

Fig. 8. Fragmentation of the M1 isovector resonance in ^{208}Pb. (A) TDA calculation; (B) RPA and (C) experimental values ref. [16]).

TABLE 1

Values of the width $\sigma = \sqrt{\mu^{(2)}}$ (the parameter c is used in eq. (26))

Calculation		Width (keV)
RPA	$c = 0$	215
	$c = 1$	238
TDA	$c = 0$	76
	$c = 1$	82
exp.		137

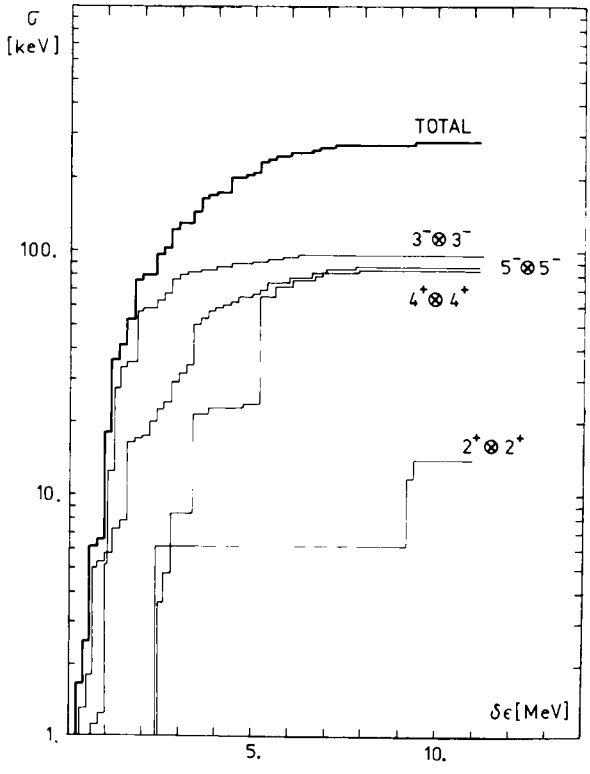

Fig. 9. Value of σ obtained with eq. (16) as a function of the distance $\delta\varepsilon$ of the fragments of M1 strength to the centroid of the distribution. The total value of σ is broken up into the contributions of the multipolarities involved in the 2p-2h configurations.

two 5^- phonons in which only one is the collective (lowest) RPA root. This is mainly due to small energy denominators in (29). The collective features enhance this effect through larger values of the corresponding vertex functions Λ_{nJ}.

The larger value of σ (RPA) as compared to σ (TDA) can be understood in terms of the greater amount of correlations that are involved in the RPA wave functions. The different time permutations of the diagrams of fig. 6E that contribute when using RPA bosons, produce the same effect of a larger set of intermediate states. The higher dimension of this space as compared to the one active in a TDA calculation is the main cause of a wider fragmentation. This effect is, for instance, much more important than the one produced by the change of the residual interaction used to construct the phonon space. In fact a change in c between $c = 0$ and $c = 1$ (cf. eq. (26C)), that encompasses a change between uncoupled isoscalar and isovector p-h modes to the introduction of isospin-violating terms of the order of $(N-Z)/A$, only causes a change in σ of a few percent.

The fact that the experimental value of σ lies in between the RPA and the TDA descriptions can also be expected since the amount of correlations in a realistic

description must be somewhat less than the ones introduced in the RPA wave functions. This, as suggested by Krison [21]), is due to the increasing number of constraints that must be imposed on the g.s. wave function to become the vacuum of all possible multipole excitations.

6. Conclusions

In the present paper we have analysed the use of the second moment of a strength distributions to gauge the coupling of a decaying state to the neighbouring configurations.

We have proved that a moment of a given order is exactly determined by the Brillouin–Wigner perturbative expansion of the decaying state up to the same order. This property allows us to define in an unambiguous way the space of intermediate states that fully determines the required moment. In particular if we consider 1p (1h) or 1p-1h coherent excitations the second moment of its fragmentation into more complex states remains determined only by 2p-1h (2h-1p) and 2p-2h states respectively.

We want here to briefly discuss the connection of the framework of the present paper with others in the existing literature. For the sake of concreteness we will restrict this discussion to the case of giant resonances in even systems.

We have already seen that within the NFT the admixture of 1p-1h and 2p-2h configurations is described by the anharmonic corrections of order $1/\Omega$ that are displayed in fig. 5. The diagram D_1 needs no special consideration since this is in general included in any realistic calculation provided that the matrix elements are evaluated with antisymmetrized states.

The contribution of the diagrams D_2 and D_3 has been analysed in several publications. In ref. [7]) the spreading width of the giant monopole resonance was calculated making use only of the diagram D_2. The value obtained was too low mainly because of the low density of 2p-2h states. The contributions of the diagrams D_2 and D_3 was seen in refs. [2,3]) to almost cancel within simplified models. This feature can also be seen in eqs. (20) since their contribution is proportional to $(q_\sigma - q_{\bar{\sigma}})^2$ that is nearly zero for multipole interactions [9]). This cancellation was however found not to be complete in ref. [6]) in which more realistic interactions were used within a shell-model approach to describe the spreading width of giant quadrupole resonances in ^{16}O and ^{40}Ca.

Both diagrams are also considered within the core-coupling RPA formalism in refs. [8,10]). The spreading width was interpreted as a consequence of the existence of an effective matrix element connecting one- and two-boson states [23]).

In this paper we have explicitly calculated such a matrix element in such a way that the diagrams D_4, D_5 and D_6 are also included. This was checked in the calculation of the corrections of order $1/\Omega$ to the energy of the one-boson state.

These vertex functions cannot in general be extended to an RPA framework as an energy-independent matrix element.

The fragmentation of the strength function of the giant M1 resonance in ^{208}Pb was analysed within the TDA and RPA calculations. The general experimental features are properly described in terms of the admixture of one- and two-boson states within both approximations. A larger fragmentation was found in RPA than in TDA as a consequence of the larger amount of correlations that are present in one framework as compared to the other. This is dominant over the changes produced by a variation of the residual interaction.

The second moment of the strength distribution does not measure the lifetime of the state. This should be estimated through its width Γ assuming a Breit–Wigner line shape that corresponds to a pure exponential decay in time.

In refs. [11,12]) the transition probabilities are obtained as a function of the excitation energy. In ref. [11]) an RPA description is used and in ref. [12]) a higher-order RPA is performed including 2p-2h states. In addition corrections of order higher than $1/\Omega$ are included due to the procedure used to consider such complicated configurations. In this respect one must be cautious with the partial inclusion of higher-order contributions since cancellations among corrections of the same order may be omitted [see e.g. cancellations among $1/\Omega^2$ terms in ref. [13])]. A calculation of the parameter Γ as a function of the excitation energy is performed in ref. [10]) with the assumption of a Breit–Wigner line shape and considering processes that are equivalent to the diagrams of fig. 6. For this purpose a smearing parameter Δ is introduced to provide for an intrinsic width of the 2p-2h intermediate states. Little is known so far about this parameter whose choice tends to wash out or enhance the fine structure of the giant resonance. The approach of the present paper may present in this respect an advantage since it needs no *ad hoc* assumption of that kind. It is worth noting that the parameter that is usually reported in the experimental studies of giant resonances is the full width at half maximum. This can directly be related to theoretical values of $\mu^{(2)}$ obtained in calculations in which the space of intermediate states has been truncated with any reasonable assumption. The present approach may prove also to be useful if the second moment is used as a higher-order energy-weighted sum rule. The value σ (TDA) can then be used to provide a rigorous and simple method to calculate lower bounds to the fragmentation that can be expected experimentally.

References

1) M. Baranger, Nucl. Phys. **A149** (1970) 225
2) G. Bertsch, Phys. Lett. **37B** (1971) 470
3) H. Ui, Proc. Conf. on new giant resonances (Sendai, Japan, 1975), p. 205
4) C.A. Engelbrecht and H.A. Weidenmüller, Nucl. Phys. **A184** (1972) 385
5) W.L. Wang and C.M. Shakin, Phys. Rev. **C5** (1972) 1898
6) T. Hoshino and A. Arima, Phys. Rev. Lett. **37** (1976) 266

7) S. Adachi and S. Yoshida, Nucl. Phys. **A306** (1978) 53
8) J.S. Deheza, S. Krewald, J. Speth and A. Faessler, Phys. Rev. **C15** (1977) 1858
9) G. Bertsch, P.F. Bortignon, R.A. Broglia and C.H. Dasso, Phys. Lett. **80B** (1979) 161
10) P.F. Bortignon and R.A. Broglia, Nucl. Phys. **A371** (1981) 405
11) S. Shlomo and G. Bertsch, Nucl. Phys. **A243** (1975) 507
12) V.G. Soloviev, Ch. Stoyanov and A.V. Vdovin, Nucl. Phys. **A288** (1977) 376;
V.G. Soloviev and Ch. Stoyanov, Nucl. Phys. **A382** (1982) 206
13) D.R. Bes, R.A. Broglia, G.G. Dussel, R.J. Liotta and R.P.J. Perazzo, Nucl. Phys. **A260** (1976) 77;
D.R. Bes, R.A. Broglia, G.G. Dussel, R.J. Liotta and H.M. Sofía, Nucl. Phys. **A260** (1976) 27
14) A. Bohr and B. Mottelson, Nuclear structure, vol. 1 (Benjamin, New York, 1969) ch. 2, p. 302
15) G.F. Bertsch, Nucl. Phys. **A354** (1981) 157
16) R.M. Laszewski, R.J. Holt and H.E. Jackson, Phys. Rev. Lett. **38** (1977) 813;
R.J. Holt, H.E. Jackson, R.M. Laszewski and J.R. Specht, Phys. Rev. **C20** (1979) 93;
S. Raman, in Neutron capture gamma-ray spectroscopy, ed. R.E. Chrien and W.R. Kane (Plenum Press, NY, 1979) p. 193;
D.J. Horen, in Proc. Giant Multipole Topical Conf., Oak Ridge 1979, ed. E. Bertrand (Horwood, 1980) p. 299
17) G.E. Brown and S. Raman, Comm. on Nucl. Part. Phys. **9** (1980) 79
18) M. Rho and G.E. Brown, Comm. on Nucl. Part. Phys. **10** (1981) 201
19) A. Bohr and B. Mottelson, Phys. Lett. **100B** (1981) 10
20) G.G. Dussel, R.P.J. Perazzo and S. Reich, Phys. Rev. **C22** (1980) 292
21) M.W. Kirson, The structure of nuclei (IAEA, Vienna, 1972) p. 257
22) D.R. Bes, R.A. Broglia and B. Nilsson, Phys. Reports **16C** (1975) 1
23) G. Brown, J.S. Deheza and J. Speth, Nucl. Phys. **A330** (1979) 290
24) R. Liotta and C. Pomar, Nucl. Phys. **A382** (1982) 1, and references therein
25) O. Bohigas, A.M. Lane and J. Martorell, Phys. Reports **51C** (1979) 267